A Novel Event Detection Method Using PMU Data with High Precision

Mingjian Cui, *Senior Member, IEEE,* Jianhui Wang, *Senior Member, IEEE,* Jin Tan, *Member, IEEE,* Anthony R. Florita, *Member, IEEE,* and Yingchen Zhang, *Senior Member, IEEE*

***Abstract*—To take full advantage of the considerably high reporting rate of phasor measurement units (PMU) data, this paper develops a novel PMU-based event detection methodology. Considering the huge amount of streaming PMU data, a data compression algorithm, swinging door trending (SDT), is first used to compress the PMU data and generate multiple compression intervals. Then dynamic programming is utilized to solve the optimization problem, which is recursively constituted by a score function. Based on predefined PMU event rules, dynamic programming merges adjacent compression intervals with the same slope direction. Finally, all the PMU event features are characterized. A conventional wavelet-based event detection method is compared with the developed dynamic programming based SDT (DPSDT) method. Numerical simulations on the real-time and synthetic PMU data show that the DPSDT method can accurately detect the start-time of an event and the event placement with relatively high precision. Also, the PMU event features, including the magnitude and duration of strokes, are characterized.**

***Index Terms*—Dynamic programming, phasor measurement unit (PMU), swinging door trending, wavelet.**

I. Introduction

WITH the wide implementation of wide area measurement systems (WAMS) in the last decade, phasor measurement units (PMUs) are able to provide measurements of electrical signals such as the voltage, current and frequency for control room applications. Signals measured by PMU are expected to have a considerably precise reporting rate, which can be 30-120 times per second [1], [2] (e.g., 30 Hz in [3], 50 Hz in [4], 60 Hz in [5], 100 Hz in [6]). Real-time PMU event detection can contribute to numerous applications in power system operations, such as the wide-area protection, state estimation, closed-loop control, and dynamic monitoring. Since the artificially simulated power system models cannot be absolutely accurate compared to the real systems, PMU-based applications are increasingly attractive as "model-free" methods [7]–[10].

There have been significant research contributions on the PMU-based event detection in recent years [11]–[13]. Generally, the event detection methods can be divided into two categories: statistical analysis and signal processing methods. As for statistical analysis methods, Xie *et al*. [3] utilized the principal component analysis (PCA) to reduce the dimensionality of the original streaming PMU data. Guo *et al*. [14] presented the PCA method for islanding detection using the PMU data for system monitoring. Gadde *et al*. [15] combined the PCA and discrete cosine transform to compress the critical disturbance information of PMU data with high fidelity. Bhui *et al*. [16] utilized the recurrence quantification analysis (RQA) to locate power system events. Biswal *et al*. [17] adopted the k-nearest neighborhood (kNN) to select the best set of features of the disturbance types in the time-frequency domain. As for signal processing methods, Kim *et al*. [5] presented a wavelet-based detection algorithm on discrete samples of collected PMU data. Jena *et al*. [18] utilized the empirical model decomposition (EMD) to assess the power system disturbance by using wide-area postdisturbance records. However, the performance of the current PMU event detection methods highly depends on the size of the sample length of moving windows. These methods cannot show the precise start-time of PMU-based events. This may lead to the loss of the detailed information between moving windows and cannot take full advantage of the considerably high reporting rate of PMU data.

Recently, to avoid the computational complexity, data compression techniques have been used to process the huge streaming amount of PMU data. Zhang *et al*. [6] utilized the swinging door trending (SDT) compression method to design an adapted protocol for WAMS. Sousa *et al*. [19] presented the singular value decomposition to compress the real data from metering devices at different substations. However, these papers mainly focus on data compression and do not solve the event detection problem.

For PMU event detection, it is important to identify the start-time of a system event for power system analysis. The precise detection of the event start-time can help operators take timely measures so that both voltage and frequency can present slight fluctuations. A pre-detected start-time of an event would cause false alarms with unnecessary operations, which possibly decreases the economic benefits of power systems. A post-detected start-time of an event would do severe damage to electrical equipments, which decreases not only economic benefits but also reliability benefits of power systems. To bridge the gap in the PMU-based event detection, this paper seeks to address two critical questions for power system operators. Is it possible to determine the precise start-time information of one PMU event? How to characterize PMU-based events so that operators can make more effective measures to mitigate them. To this end, this paper develops a novel PMU-based event detection method, i.e., dynamic

M. Cui and J. Wang are with the Department of Electrical Engineering at Southern Methodist University, Dallas, TX, 75275 USA (email: {mingjiancui, jianhui}@smu.edu).

J. Tan, A. R. Florita, and Y. Zhang are with the National Renewable Energy Laboratory (NREL), Golden, CO, 80401 USA (email: {jin.tan, anthony.florita, yingchen.zhang}@nrel.gov).

Manuscript received, 2018.

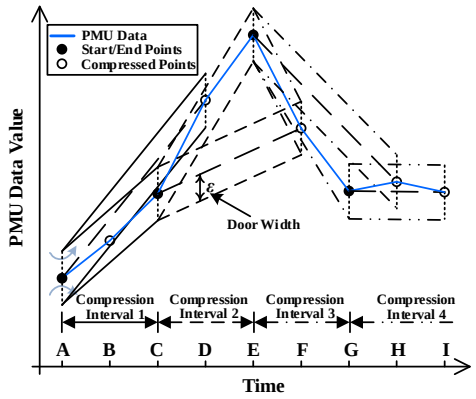

Fig. 1. Schematic of the SDT algorithm.

programming-based SDT (DPSDT), to identify events and characterize their features. The main contributions of the developed method are that: (i) it can accurately detect the start point of a PMU-based event; and (ii) it can also reduce the false alarms that are challenge for most of state-of-the-art methods. The specific tasks of this paper include: (i) using the SDT compression method and dynamic programming to precisely detect the start-time and placement of PMU-based events; and (ii) characterizing the event features of magnitude and duration through the first downward and upward strokes.

The organization of this paper is as follows. In Section II, the SDT compression method is briefly introduced. Section III presents the recursion methodology of dynamic programming based on the SDT compression intervals. Section IV described the evaluation metrics to validate the effectiveness of DPSDT. Case studies and result analysis performed on publicly real-time and synthetic PMU data are discussed in Section V. Concluding remarks are summarized in Section VI.

II. Swinging Door Trending

The SDT compression method has been widely used to compress the PMU data for the WAMS [6] and the smart meters data in electrical distribution systems [19]. This algorithm is originally proposed by Bristol [20] for data compression and recently used in power systems. It is based on the concept of a "swinging door" with a "hinge" or "pivot point" whenever the next point in the time series causes any intermediate point to fall outside the area partitioned by the compression interval bounds. The compression interval bounds are defined by the door width (ε), which is the only tunable parameter in the SDT. As can be seen in Fig. 1, multiple compression intervals are segregated by the SDT algorithm. Taking the first compression interval as an example, A is first set as the start point and C is stored as the end point by the SDT blanket A–D. Then, points A, B, and C are represented by the straight line from A to C. Finally, points B, D, and F are compressed inside the compression bounds determined by points C, E, G, respectively. The compression intervals are segregated as A–C, C–E, and E–G.

III. Dynamic Programming Based SDT

Based on the segregated compression intervals, a dynamic programming approach is used to detect the PMU-based event from the perspective of constituting an optimization model. The main idea is to merge adjacent compression intervals that have the same slope direction into one combined compression interval. The PMU-based event is detected by the predefined event rules: the magnitude rule and the slope rate rule, which are described in Section III-A. Then the maximum objective function is built and solved by the dynamic programming method via a score function in Section III-B.

A. PMU Event Rules

1) Definitions of Magnitude and Slope Rate Rules: The PMU-based event rules are predefined by users and required for the developed detection method. Generally, one PMU event consists of upward and downward strokes, i.e., $E = \{ST_1, \cdots, ST_m, \cdots\}$, where $ST_m = (s_m, e_m)$ represents the *m*th stroke with the corresponding start (s_m) and end (e_m) points. Taking the frequency data as an example, the PMU-based event with a downward stroke first occurring is usually caused by the abrupt lack of positive power such as unexpected generator tripping events. The PMU-based event with an upward stroke first occurring is usually caused by the abrupt lack of positive load such as unexpected load shedding events. The magnitude rule checks whether the magnitude has increased (or decreased) by a specified threshold, Tr_{mag}, and defined as:

$$R_{\text{mag}} = 1, \quad if \quad |p_{s_m} - p_{e_m}| > Tr_{\text{mag}} \tag{1}$$

The slope rate rule checks whether the rate of increase (or decrease) is greater than a specified threshold, Tr_{slo}, given by:

$$R_{\text{slo}} = 1, \quad if \quad (|p_{s_m} - p_{e_m}|)/(e_m - s_m) > Tr_{\text{slo}} \tag{2}$$

where p represents the measured PMU data.

2) Determination of Magnitude and Slope Rate Thresholds: Both the magnitude threshold in (1) and slope rate threshold in (2) can be automatically determined from the historical measured dataset of voltage and frequency under the normal operating condition. First, operators can readily gather the maximum magnitude $M_{\text{max}}^{\text{Norm}}$ and slope rate $S_{\text{max}}^{\text{Norm}}$ from the normal operating dataset. However, due to the impact of the ambient noise, the maximum magnitude and slope rate may change along with the corresponding normal operating dataset that operators choose. Thus, a tolerance value is added and defined as a small proportion of the maximum magnitude $M_{\text{max}}^{\text{Norm}}$ and slope rate $S_{\text{max}}^{\text{Norm}}$. Finally, we can get the formulations of the magnitude and slope rate thresholds, given by:

$$Tr_{\text{mag}} = M_{\text{max}}^{\text{Norm}} + \underbrace{\phi_{\text{mag}} \times M_{\text{max}}^{\text{Norm}}}_{Tolerance\ Value} \tag{3}$$

$$Tr_{\text{slo}} = S_{\text{max}}^{\text{Norm}} + \underbrace{\phi_{\text{slo}} \times S_{\text{max}}^{\text{Norm}}}_{Tolerance\ Value} \tag{4}$$

where ϕ_{mag} and ϕ_{slo} are the tolerance coefficients of the magnitude and slope rate thresholds, respectively. Based on

the experimental experience, ϕ_{mag} and ϕ_{slo} can be chosen in the range of 10%–20%.

B. Dynamic Programming

Dynamic programming is a method for solving a complex problem by breaking it down into a collection of simpler subproblems [21]. The compression intervals detected by SDT comply with the same event rules, as described in Section III-A.

First, the compression intervals that satisfy the ramp rules are rewarded by a score function; otherwise, their score is set to zero. An increasing length score function S is designed based on the length of the intervals segregated by the SDT. Given a time interval $(i,\ j)$ of discrete time points of PMU data and a time point k located into this interval (i.e., $i<k<j$), the score function should conform to a super-additivity property, given by:

$$S(i,j) > S(i,k) + S(k,j), \quad \forall k : i<k<j \tag{5}$$

A family of score functions can satisfy this property. In this paper, the score function presented in [22], [23] is adopted and given by:

$$S(i,j) = (i-j)^2 \times R(i,j) \tag{6}$$

where $R(i,j)$ represents the magnitude rule in (1) and the slope rate rule in (2), i.e., $R \in \{R_{\text{mag}}, R_{\text{slo}}\}$. Then, an objective function J is constituted according to the dynamic programming, given by:

$$J(i,j) = \max_{i<k<j} [S(i,k) + J(k+1,j)] \tag{7}$$

Based on (5)–(7), the process of solving the optimization problem can proceed recursively as follows. Assuming that the number of strokes is M, the PMU data event consists of multiple upward and downward strokes, i.e., $E = \{ST_1, \cdots, ST_m, \cdots\}$; and compression intervals of the PMU data under normal operations do not present any strokes, i.e., $\overline{E} = \{\overline{ST_1}, \cdots, \overline{ST_m}, \cdots\}$. For the mth compression interval without strokes, i.e., $\overline{ST_m} = (\overline{s_m}, \overline{e_m})$, the event rules, the score function, and the objective function of the dynamic programming can respectively be calculated as:

$$R_{\text{mag}}(i,j) = R_{\text{slo}}(i,j) = 0, \quad \forall i,j : \ \overline{s_m} < i < j < \overline{e_m} \tag{8}$$

$$S(i,j) = 0, \quad \forall i,j : \ \overline{s_m} < i < j < \overline{e_m} \tag{9}$$

$$J^*(\overline{s_m}, \overline{e_m}) = 0, \quad \forall m : \ 1 \le m < M \tag{10}$$

For the mth compression interval with a PMU data event, i.e., $ST_m = (s_m, e_m)$, the event rules, the score function, and the objective function of the dynamic programming can respectively be calculated by:

$$R_{\text{mag}}(i,j) = R_{\text{slo}}(i,j) = 1, \quad \forall i,j : \ \overline{s_m} < i < j < \overline{e_m} \tag{11}$$

$$S(i,j) = (i-j)^2, \quad \forall i,j : \ \overline{s_m} < i < j < \overline{e_m} \tag{12}$$

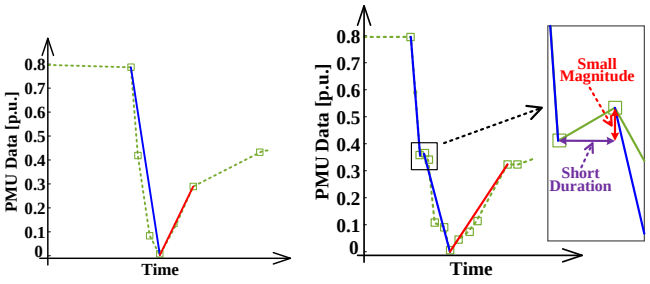

(a) An event without anomaly (b) An event with anomaly

Fig. 2. Comparison of a PMU data event with and without anomaly.

$$\begin{aligned} J^*(s_m,e_m) &= \max_{s_m<k_1<e_m} S(s_m,k_1) + J(k_1+1,e_m) \\ &= \max_{s_m<k_1<e_m} S(s_m,k_1) + \max_{k_1+1<k_2<e_m} S(k_1+1,k_2) \\ &+ \cdots + \max_{k_{i-1}+1<k_i<e_m} S(k_{i-1}+1,k_i) + J(k_i+1,e_m) \\ &= \max_{s_m<k_1<k_2<\cdots<k_{i-1}<k_i<e_m} S(s_m,k_1) + S(k_1+1,k_2) \\ &+ \cdots + S(k_{i-1}+1,k_i) + S(k_i+1,e_m) \end{aligned} \tag{13}$$

Assuming that a given PMU data series $\{p_{\overline{s_1}}, \cdots, p_{\overline{s_m}}, \cdots, p_{s_1}, \cdots, p_{s_m}, \cdots, p_{\overline{e_M}}\}$ starts without strokes at the beginning and can be presented as $\mathbf{\Theta} = \{\overline{ST_1}, \cdots, \overline{ST_m}, ST_1, \cdots, ST_m, \cdots, \overline{ST_M}\}$, the solution to (7), $J^*(\overline{s_m}, \overline{e_M})$, for the mth compression interval without strokes is expanded in (14), where this recursive process using the dynamic programming is stopped until $k_i = e_M - 1$. Considering (9) and (10), the objective $J^*(\overline{s_m}, \overline{e_M})$ can be transformed to the objective $J^*(s_{m+1}, \overline{e_M})$ of the $(m+1)$th compression interval with strokes, given by:

$$\begin{aligned} J^*(\overline{s_m}, \overline{e_M}) &= \max_{\overline{s_m}<k_1<k_2<\cdots<k_{i-1}<k_i<\overline{e_M}} J(k_i, \overline{e_M}) \\ &= J^*(s_{m+1}, \overline{e_M}) \end{aligned} \tag{15}$$

where the objective $J^*(s_{m+1}, \overline{e_M})$ is induced by (16). Considering the super-additivity in (5), the final detected event sequence of PMU data series $\{p_{\overline{s_1}}, \cdots, p_{\overline{s_m}}, \cdots, p_{s_1}, \cdots, p_{s_m}, \cdots, p_{\overline{e_M}}\}$ is solved as:

$$J^*(\overline{s_1}, \overline{e_M}) = \textstyle\sum_{m=2}^{M} S(s_m, e_m) \tag{17}$$

C. Anomaly Processing

During the recursion of dynamic programming, one of the more interesting findings is the occurrence of abnormal compression intervals [24], which are termed as "anomaly" in this paper and set as $A(i,j)$. The characteristics of an anomaly are the inverse tendency, small magnitude, and short duration, as shown in Fig. 2. An upward anomaly occurs between two downward strokes and makes the recursion of the dynamic programming abruptly break according to the strict super-additivity property in (5). The anomaly rule is first predefined based on experimental experiences. Similarly with PMU-based event rules, the magnitude of one anomaly cannot be greater

$$\begin{aligned} J^*\left(\overline{s_m},\overline{e_M}\right) &= \max_{\overline{s_m}<k_1<\overline{e_M}}\left[S\left(\overline{s_m},k_1\right)+J\left(k_1+1,\overline{e_M}\right)\right] \\ &= \max_{\overline{s_m}<k_1<\overline{e_M}}\left\{S\left(\overline{s_m},k_1\right)+\max_{k_1<k_2<\overline{e_M}}\left[S\left(k_1,k_2\right)+J\left(k_2+1,\overline{e_M}\right)\right]\right\} \\ &= \max_{\overline{s_m}<k_1<\overline{e_M}}\left\{S\left(\overline{s_m},k_1\right)+\max_{k_1<k_2<\overline{e_M}}\left\{S\left(k_1,k_2\right)+\cdots+\max_{k_{i-1}<k_i<\overline{e_M}}\left[S\left(k_{i-1},k_i\right)+J\left(k_i+1,\overline{e_M}\right)\right]\right\}\right\} \\ &= \max_{\overline{s_m}<k_1<k_2<\cdots<k_{i-1}<k_i<\overline{e_M}}\left[S\left(\overline{s_m},k_1\right)+S\left(k_1,k_2\right)+\cdots+S\left(k_{i-1},k_i\right)\right]+\max_{k_{i-1}<k_i<\overline{e_M}}J\left(k_i+1,\overline{e_M}\right) \end{aligned} \tag{14}$$

$$\begin{aligned} J^*\left(s_{m+1},\overline{e_M}\right) &= \max_{s_{m+1}<k_1<\overline{e_M}}\left[S\left(s_{m+1},k_1\right)+J\left(k_1+1,\overline{e_M}\right)\right] \\ &= \max_{s_{m+1}<k_1<\overline{e_M}}\left\{S\left(s_{m+1},k_1\right)+\max_{k_1<k_2<\overline{e_M}}\left[S\left(k_1,k_2\right)+J\left(k_2+1,\overline{e_M}\right)\right]\right\} \\ &= \max_{s_{m+1}<k_1<\overline{e_M}}\left\{S\left(s_{m+1},k_1\right)+\max_{k_1<k_2<\overline{e_M}}\left\{S\left(k_1,k_2\right)+\cdots+\max_{k_{i-1}<k_i<\overline{e_M}}\left[S\left(k_{i-1},k_i\right)+J\left(k_i+1,\overline{e_M}\right)\right]\right\}\right\} \\ &= \max_{s_{m+1}<k_1<k_2<\cdots<k_{i-1}<k_i<\overline{e_M}}\left[S\left(s_{m+1},k_1\right)+S\left(k_1,k_2\right)+\cdots+S\left(k_{i-1},k_i\right)\right]+\max_{k_{i-1}<k_i<\overline{e_M}}J\left(k_i+1,\overline{e_M}\right) \end{aligned} \tag{16}$$

than $Tr_{\text{mag}}^{\text{Anom}}$. The duration of one anomaly cannot be longer than $Tr_{\text{dur}}^{\text{Anom}}$. The mathematical formulation is given by:

$$A(i,j)=\begin{cases}1, & \text{if } |p_i-p_j|<Tr_{\text{mag}}^{\text{Anom}}\cap|j-i|<Tr_{\text{dur}}^{\text{Anom}}\\ 0, & \text{if } not\end{cases} \tag{18}$$

where $Tr_{\text{mag}}^{\text{Anom}}$ and $Tr_{\text{dur}}^{\text{Anom}}$ are determined by the experimental experience. $Tr_{\text{mag}}^{\text{Anom}}$ is chosen in the range of 0.03–0.05, and $Tr_{\text{dur}}^{\text{Anom}}$ is chosen in the range of 0.3–0.5.

To avoid the impact of anomalies, anomalies are detected and merged into the adjacent strokes by improving the score function in (6), formulated as:

$$S(i,j)=(i-j)^2\times[R(i,j)+A(i,j)] \tag{19}$$

Given the nth anomaly A_n and adjacent strokes ST_n and ST_{n+1}, the PMU data can be depicted as $\mathbf{\Theta}=\{\cdots,ST_m,A,ST_{m+1},\cdots\}$, where ST_n=(s_n,e_n), ST_{n+1}=(s_{n+1},e_{n+1}), and A_n=$(e_n+1,s_{n+1}-1)$. Finally, both the anomaly and adjacent strokes are combined into one significant stroke, given by:

$$(s_n,e_n)\leftarrow(s_n,e_{n+1}) \tag{20}$$

where the total number of strokes is reduced to M-N. N is the total number of anomalies.

The compressed PMU data processed by SDT is split into multiple overlapping moving windows. The length of each window must be longer than the longest duration of strokes, which can be characterized by the statistical analysis of distributions of stroke features. Assuming that the window length is W_{L} and the overlap between adjacent windows is W_{O}, the start and end indices of the ith window are given by:

$$s_{\text{W},i}=(i-1)\cdot(W_{\text{L}}-W_{\text{O}}) \tag{21}$$

$$e_{\text{W},i}=i\cdot W_{\text{L}}-(i-1)\cdot W_{\text{O}} \tag{22}$$

The application of DPSDT will yield the set of strokes of PMU-based events for each windowed PMU data signal, i.e., $ST_{s_{\text{W},1}:e_{\text{W},1}},\cdots,ST_{s_{\text{W},i}:e_{\text{W},i}},\cdots,ST_{s_{\text{W},M}:e_{\text{W},M}}$. The longest strokes are determined by merging the strokes that are located in the overlap of adjacent windows.

Algorithm 1: Dynamic Programming Based Swinging Door Trending Algorithm

```
Compressing PMU data p by SDT into L intervals:
L ← length(p)
Initializing score function of zero length intervals:
for Iteration n from 1 to L do
    J(n,n) ← 0
end
Computing maximum scores for intervals in the same direction based on PMU event rules:
for Iteration n from 2 to L do
    for Iteration i from 1 to (L−n+1) do
        j ← i+n−1
        for Iteration k from i to (j−1) do
            Anomaly processing:
            for Iteration ii, kk from i to k do
                if |p_ii − p_kk| < 0.05 ∩ |kk − ii| < 0.5 then
                    S(i,k) ← (i−k)^2 × [R(i,k)+A(i,k)]
                else
                    S(i,k) ← 0
                end
            end
            q ← S(i,k) + J(k,j)
            Saving indices until maximum scores:
            if q < J(i,j) then
                J(i,j) ← q; K(i,j) ← k
            end
        end
    end
end
```

D. Procedure of the Developed DPSDT Method

To solve the optimization problem constituted in (7), a simple standard recursion is given in Algorithm 1 with pseudocode. The flowchart of the developed PMU-based event

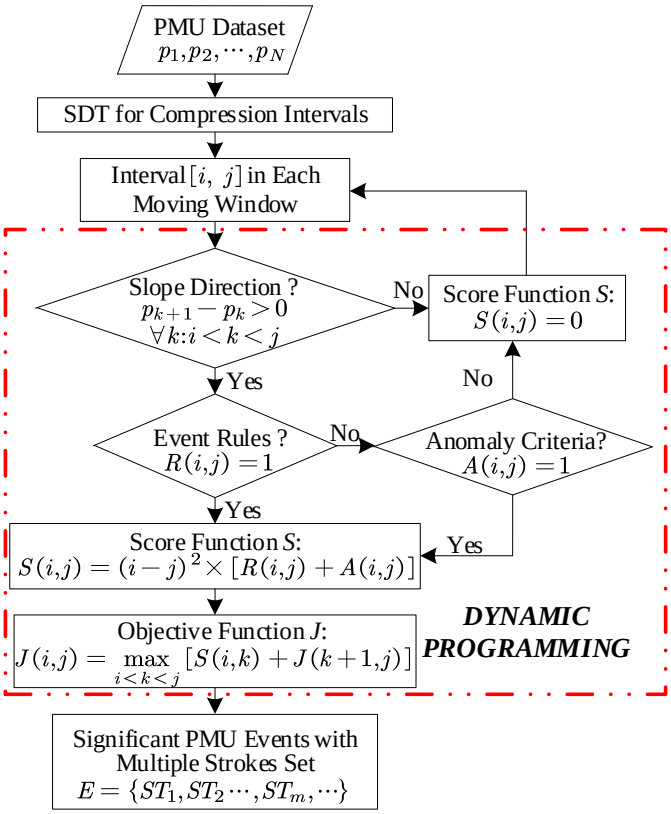

Fig. 3. Flowchart of the developed PMU-based event detection methodology.

detection methodology is shown in Fig. 3. Three major steps are briefly summarized, including:

- ***Step 1***: The real-time or synthetic PMU data is first compressed into multiple compression intervals using the SDT.
- ***Step 2***: Based on the PMU event rules, dynamic programming combines compression intervals with the same slope direction. If intervals do not conform to event rules, anomalies are identified and combined to the score function. Then, the objective with the maximum score is obtained.
- ***Step 3***: The set of significant strokes are detected and combined as the final detected PMU events. Evaluation metrics introduced in the following section are calculated based on the detected events for mining more practical information, such as the event placement.

IV. Evaluation Metrics for Comparison

A. Metrics I

For the simplicity of comparison, the normalized wavelet energy (NWE) is used to validate the effectiveness of the developed DPSDT method. NWE is defined to calculate the root mean square value of detailed wavelet coefficients in a moving window. Detailed information about NWE can be found in [4], [5]. The formulation is given by:

$$NWE\left(i; N_{\mathrm{W}}, N_{\mathrm{L}}, N_{\mathrm{C}}\right) = \frac{MWE\left(i; N_{\mathrm{W}}, N_{\mathrm{L}}, N_{\mathrm{C}}\right)}{MWE\left(i; N_{\mathrm{W}}, N_{\mathrm{H}}, N_{\mathrm{C}}\right)} \quad (23)$$

where i is the data point in the designed moving window and $i = 1, 2, \cdots, N_{\mathrm{W}}$. N_{W} is the number of samples in the moving window. N_{L} is the number of wavelet decomposition levels. N_{C} is the number of coefficients in each decomposition level. N_{H} is the total number of samples in one hour. MWE is the modified wavelets energy (MWE) metric, given by:

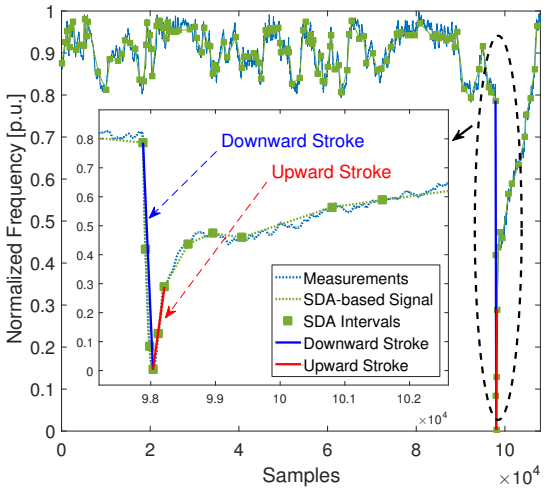

Fig. 4. Detection results of measured PMU data of frequency with a significant trip event at the Harris substation.

$$MWE\left(i; N_{\mathrm{W}}, N_{\mathrm{L}}, N_{\mathrm{C}}\right) = \sqrt{\frac{1}{N_{\mathrm{W}}} \sum_{j=1}^{N_{\mathrm{L}}} \sum_{k=1}^{N_{\mathrm{C}}} \left|d_{j,k}\left(i\right)\right|^2} \quad (24)$$

where $d_{j,k}$ is the detailed coefficient calculated by the inner product between the signal and wavelet function, which can be obtained by the wavelet decomposition. There are multiple wavelet families for designed mother wavelets. In this paper, the typical Daubechies wavelet "DB 1" is deployed for case studies because the "DB 1" wavelet presents the highest time-localized wavelet among all Daubechies wavelet series [5]. The window length N_{W} is set as 16 samples (≈0.53 s). The number of wavelet decomposition levels N_{L} is set as 3.

B. Metrics II

Another set of metrics is used to evaluate the performance of fault clearance using different detection methods. According to Ref. [25], the security limit of maximum voltages should be less than 1.1 p.u.. Thus, the rate of buses with out-of-limit voltage ($ROLV$) is defined as the number of buses with out-of-limit voltage accounting for the total number of buses in the system. In addition, the security and quality of supply standards (SQSS) [26] requires frequency change to be maintained within ±0.2 Hz of the nominal frequency. Thus, the rate of buses with out-of-limit frequency ($ROLF$) is defined as the number of buses with out-of-limit frequency accounting for the total number of buses. Another two metrics are defined as the mean time of the maximum bus voltage ($MTMV$) and mean time of the maximum bus frequency ($MTMF$) during the restoration process. Overall, smaller $ROLV$ and $ROLF$ mean that the system can keep a more secure operation after using control actions, while smaller $MTMV$ and $MTMF$ mean that the system can restore to its normal operating condition more quickly.

V. Case Studies and Results

A. PMU Data Description and Preprocessing

Two different sets of realistic and synthetic PMU data are utilized to illustrate the efficacy of the developed detection method. First the real-world synchrophasor data of the Texas Synchrophasor Network [27], [28] was sampled at four PMU locations at McDonald Observatory (MCD, West Texas), Harris (Austin), Baylor (near Dallas), and University of Texas Pan American (UTPA, South Texas), respectively. The PMU data spans from 11:00:00 PM to 12:00:00 PM on July 10$^{\text{th}}$ 2016. PMUs are used to collect the synchrophasor data of the frequency with a 30 Hz sampling rate. The second synthetic PMU data is generated by the Siemens PSS/E 23-bus system [29] with ground fault events on each bus. The PMU data consists of frequency, voltage, active/reactive power, and phase angle. Overall, the first dataset is used to verify the effectiveness of the developed DPSDT method, and the second dataset is used for statistical analysis. All the PMU data are preprocessed and normalized by:

$$\tilde{p} = (p - p_{\min})/(p_{\max} - p_{\min}) \tag{25}$$

where $p_{\min}$ and $p_{\max}$ are the minimum and maximum values of the measured PMU data, respectively. $\tilde{p}$ is the normalized value of the PMU data.

B. Detailed Analysis of one PMU Location

To verify the effectiveness of the developed DPSDT method, another method that has been widely used for the PMU event detection [4], [5] is adopted for comparison. The information on the two methods is described as follows:

- **Method 1:** wavelet-based event detection (WED) method based on the NWE metric.
- **Method 2 (*proposed*):** dynamic programming-based swinging door trending (DPSDT) method.

Fig. 4 shows the detection results by using the developed DPSDT method for the frequency data at the Harris substation. The door width of the SDT is set as 0.02 p.u. As can be seen, the power system is operated under normal circumstances during the first half part of the signal though some slight fluctuations occur. As for the latter half part of the signal, there is a trip event of frequency with a significant downward stroke in a very short time. The stroke magnitude can be roughly estimated as over 0.7 p.u. This strip of frequency signal is mainly caused by the real power event, such as generator trips or automated control. To precisely detect this event, the developed DPSDT method first segregates the frequency signal into multiple compression intervals marked by the green rectangles. Then, a pair of downward (see the solid blue line) and upward (see the solid red line) strokes are identified by the dynamic programming using the signal of SDT-based compression intervals (see the dashed green line).

Fig. 5 shows detailed coefficients that are relevant to d_0, d_1, and d_2. Comparing coefficients with the original frequency signal in Fig. 4, there is a significant decrease through d_0, d_1, and d_2 for the 19$^{\text{th}}$ segment by using both WED and DPSDT. This coefficients decrease is caused by the change

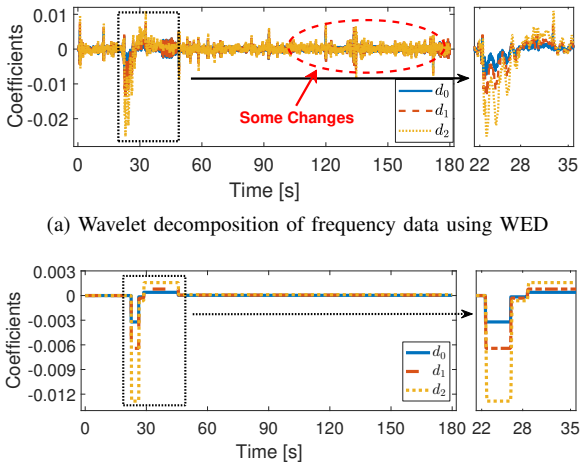

(a) Wavelet decomposition of frequency data using WED

(b) Wavelet decomposition of frequency data using DPSDT

Fig. 5. Wavelet decomposition of frequency data provided in Fig. 4 for the 19$^{\text{th}}$ segment with three coefficients: d_0, d_1, and d_2.

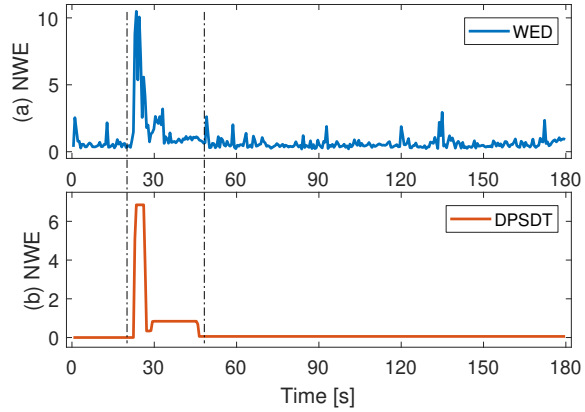

Fig. 6. Comparison of NWE metric for (a) WED and (b) DPSDT.

TABLE I
Comparison of Start-Times of the PMU-Based Event at Multiple Substations

Substations	WED in [4], [5]		DPSDT (*proposed*)	
	Minute	Second	Minute	Second
Harris	54	22.79	54	22.6999
MCD	54	22.79	54	22.5333
Baylor	54	22.26	54	22.5667
UTPA	54	22.79	54	22.9001

in the frequency signal. From the observation of coefficients, WED also shows some changes at the latter part of the 19$^{\text{th}}$ segment, which may mislead users to detect the fake PMU event as the real one. Whereas DPSDT can clearly present the significant coefficients change. For a better illustration, Fig. 6 compares the NWE metrics calculated by WED and DPSDT, respectively. The NWE signal using WED shows a significant increase but with too much noise, which makes it challenging to detect the exact PMU event. The NWE signal using DPSDT can clearly present a significant increase and help users readily locate this event.

TABLE II
EVENT FEATURES DETECTED AT MULTIPLE PMU SUBSTATIONS

Event Features		Harris	MCD	Baylor	UTPA
Magnitude [Hz]	Down Stroke	0.1843	0.1759	0.1781	0.1940
	Up Stroke	0.0673	0.0989	0.0981	0.0789
Duration [s]	Down Stroke	5.1333	3.7001	4.0667	4.3667
	Up Stroke	*5.9001*	*16.9667*	*17.0667*	*6.4333*
Slope [Hz/s]	Down Stroke	0.0359	0.0475	0.0438	0.0444
	Up Stroke	0.0114	0.0058	0.0057	0.0123

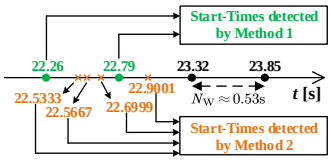

Fig. 7. Comparison of start-times of the PMU-based event at four substations.

C. Results and Analysis of Multiple PMU Locations

The most important advantage of the developed DPSDT method is that it can detect a PMU-based event with a high time resolution. Table I compares the start-time of the PMU-based event at four substations. As can be seen, both WED and DPSDT can detect this event at the minute level, i.e., 54 min. However, with regard to the second level, WED can only detect a PMU event occurring at either 22.79 s or 22.26 s. It cannot detect any detailed start-time information with a higher time resolution. This is because WED utilizes the NWE metric which is calculated by the moving window with the length of $N_W = 16$ samples (≈0.53 s). The start-time detected by WED can only be determined as $n \times N_W$, where n is a positive integer. This finding can be clearly illustrated by Fig. 7. Overall, it indicates that the WED method cannot adapt to the PMU data with a considerably high reporting rate, which has been significantly updated by advanced PMU equipments in recent years.

Another important advantage of the DPSDT method is that it can characterize the main PMU event features, including the magnitude, duration, and slope of the downward and upward strokes. However, it is very challenging for the WED to provide information on these event features for power system operators. Table II shows the numerical results of different PMU event features at four substations. In this case study, the downward and upward stroke magnitudes are in the ranges of 0.17–0.20 Hz and 0.06–0.10 Hz, respectively. The downward and upward stroke durations are in the ranges of 4.06–5.14 s and 5–18 s, respectively. The downward and upward stroke slopes are in the ranges of 0.03–0.05 Hz/s and 0.005–0.013 Hz/s, respectively. Most event features are with relatively robust variations of standard deviations 0–0.6. Whereas the upward stroke duration presents a large variation of standard deviation 6.27. Generally, the downward stroke represents the event generating process and the upward stroke represents the event recovery process. Hence, it is possible to accurately characterize the event generating process by using the developed DPSDT method. Whereas it is still challenging to characterize the event recovery duration, which highly depends on different event clearing measures.

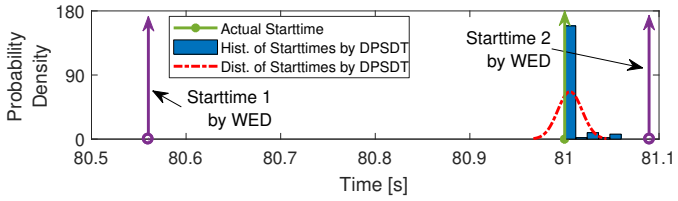

Fig. 8. Comparison of start-times of a fault event on Bus #101 based on PMU data simulated from 197 channels.

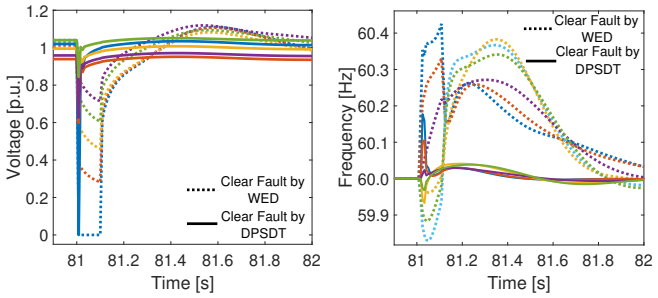

(a) Voltage data (b) Frequency data

Fig. 9. Comparison of the fault clearance using different detection methods on five representative buses.

D. Analysis of PMU Event Features

Assuming that bus fault events are preset at 81 s in the simulated Siemens PSS/E 23-bus system, there are totally 23 fault events separately simulated on each system bus and 197 channels (for each bus: 23×3 voltage, angle, and frequency; for each line: 64×2 active/reactive power) are used to generate 4,531 (23×197) sets of data points of system events. To mimic the realistic PMU data, the noise signal with a signal-to-noise ratio of 92 dB [3] is appended to the synthetic simulated PMU data for different events. For the statistical analysis, Fig. 8 shows the actual start-time (the green arrow), start-time detected by WED (purple arrows), and start-time detected by DPSDT. All the start-times detected by DPSDT are plotted in the blue histogram and the red distribution curve, respectively. Similarly to the results in Section V-C, the DPSDT can detect the bus fault events with a significantly high precision (≈81.0333 s).

Table III compares the detected start-time information using different methods, including PCA, WED, RQA, kNN, EMD, and DPSDT. The real start-time of this event is at 81 s. Measurements on Buses #101, #102, #151, and #152 are used to testify the effectiveness of different methods. It is shown that the developed DPSDT method detects the most accurate start-time with the smallest time difference in the range of 0.0333–0.0416 s. For the PCA, WED, kNN, and EMD, the time difference is in the range of 0.09–0.2233 s, which is relatively larger than that detected by DPSDT. The moving window in these methods is set as 16 samples (≈0.1333 s). The RQA method detects the largest time difference 0.2567 s. This is because RQA quantifies the number and duration of recurrences of a dynamical system [16] and a longer moving window is set as 20 samples (≈0.1667 s).

Fig. 9 compares the efficacy of fault clearance using DPSDT and WED methods on five representative buses, respectively. By using the detailed start-time information provided by

TABLE III
COMPARISON OF START-TIME DETECTED BY DIFFERENT METHODS WITH THE REAL START-TIME AT 81 S

Methods	#101	#102	#151	#152
PCA	81.09	81.09	81.09	81.2233
WED (wavelet)	81.09	81.09	81.09	81.09
RQA	81.2567	81.2567	81.2567	81.2567
kNN	81.09	81.09	81.09	81.2233
EMD	81.09	81.09	81.09	81.2233
DPSDT	81.0333	81.0333	81.0333	81.0416

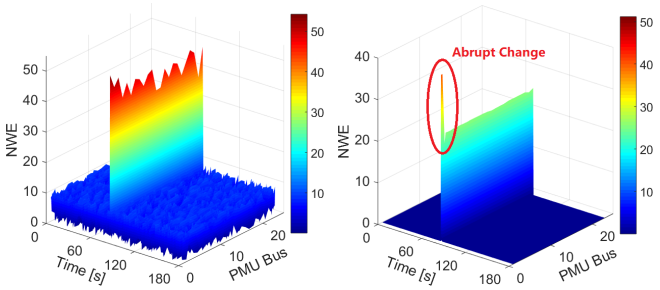

(a) Voltage with a fault on Bus #101 (b) Voltage with a fault on Bus #101

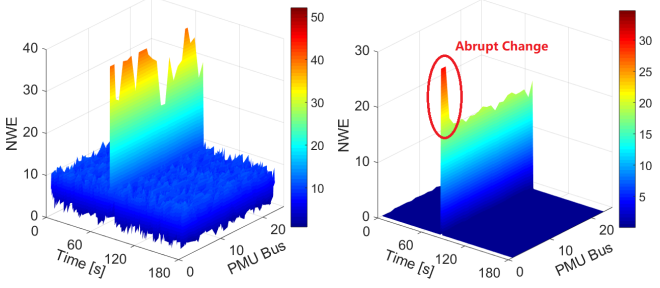

(c) Frequency with a fault on Bus #101 (d) Frequency with a fault on Bus #101

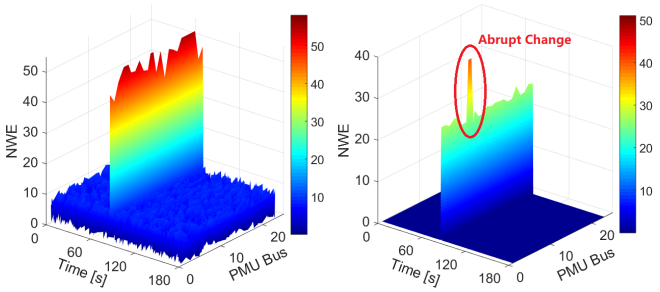

(e) Voltage with a fault on Bus #202 (f) Voltage with a fault on Bus #202

Fig. 10. Comparison of NWE metrics for the voltage and frequency data with a bus fault using: WED (left column) and DPSDT (right column).

DPSDT, the bus faults are cleared instantly (in $\Delta t \approx$81.0333-81=0.0333 s) with slight fluctuations for both voltage and frequency data, which can contribute to the stable operations of power systems. For the start-time information provided by WED, the bus faults are cleared in $\Delta t \approx$81.09-81=0.09 s, which is a longer time delay and renders both voltage and frequency data much more fluctuating. This phenomenon makes it challenging to apply WED into power systems, specially for the wide-area protection [30] and closed-loop control [31].

Fig. 10 compares NWE metrics for the voltage and frequency data using WED and DPSDT methods. The bus faults

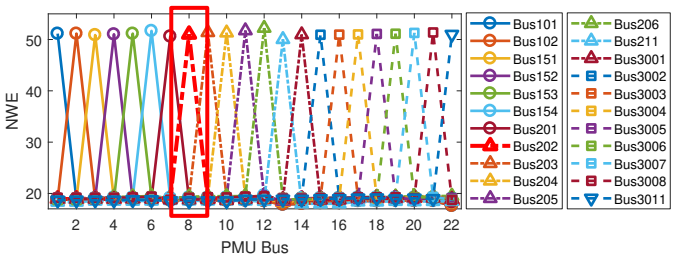

Fig. 11. NWE metrics of the voltage data for bus faults separately simulated on each bus at time 81.0333 s.

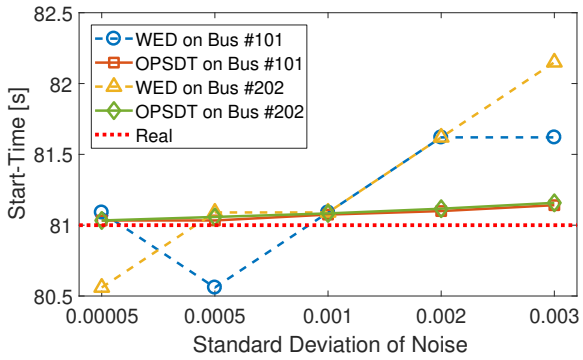

Fig. 12. Comparison of the impacts of different ambient noise on the event start-time using WED and DPSDT.

are set on Bus #101 (the 1st bus) in Figs. 10a–10d and Bus #202 (the 8th bus) in Figs. 10e–10f, respectively. For all cases, both WED and DPSDT are capable of identifying the outliers in NWE around the 81st second, whereas the proposed DPSDT method can explicitly detect the bus fault event (see the blue area in Fig. 10) without the impact of irregular NWEs under normal conditions. Another interesting finding is that it is possible to expand the DPSDT method as a PMU-based fault location technique. Compared Figs. 10a and 10c with Fig. 10e, the NWE metrics calculated by WED do not present evident distinctions on different system buses. Thus, it is still challenging for operators to know where the bus fault is located. This is because the WED method can only characterize abrupt changes with large magnitude in wavelet coefficients, but it cannot quantify the level of each abrupt change by just shrinking the noise. Unlike the WED, DPSDT is able to highlight the data with events and totally neglect the data noise. As can be seen in Figs. 10b and 10f, the fault events cause the electrical signals on the faulted bus with the largest NWE value, which is vividly characterized by the proposed DPSDT method. Hence, the location of a faulted bus is successfully identified based on the PMU data.

For a better illustration, Fig. 11 shows all the NWE metrics of the voltage data for bus faults separately simulated on each bus at time 81.0333 s. It is shown that NWE metrics of most buses, where the fault event is not simulated, are approximately 20. For the NWE metrics that are approximately 50, it is readily used to identify the faulted bus. Taking the red dashed line as an example, a bus fault is simulated on Bus 202 (the 8th bus). The NWE based on the DPSDT accurately illustrates the eighth bus with the largest value ($\approx$50).

To analyze the impact of ambient noise, the measured

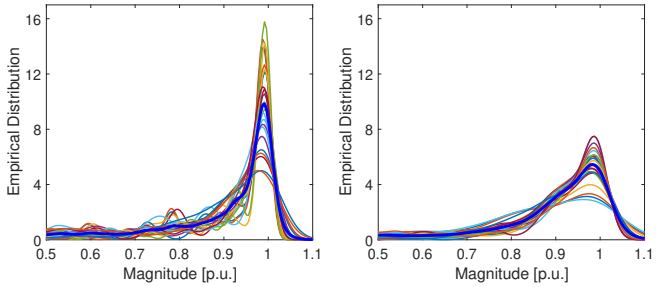

(a) Up-Stroke Magnitude (b) Down-Stroke Magnitude

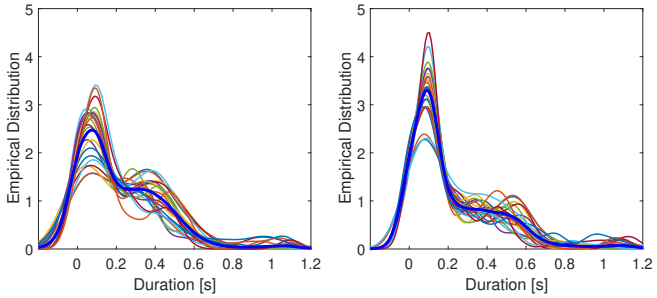

(c) Up-Stroke Duration (d) Down-Stroke Duration

Fig. 13. Empirical distributions for up- and down-strokes of PMU-based events. The superimposed blue line shows the mean histogram of averaging over every bus fault event (totally 23) and sampling channel (totally 197).

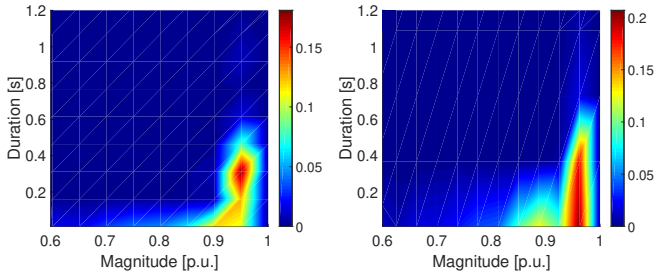

(a) Upward strokes (b) Downward strokes

Fig. 14. Joint distributions of magnitude and duration for up- (left) and down-strokes (right).

voltage and frequency data is assumed to be corrupted by a Gaussian noise with zero mean and multiple standard deviations (0.00005, 0.0005, 0.001, 0.002, and 0.003). Fig. 12 shows the impacts of different ambient noise on the event start-time using WED and DPSDT. As can be seen, the start-time detected by WED (dashed blue and yellow lines) is significantly sensitive to the ambient noise with the large and fluctuating distance to the real start-time (dashed red line). The corresponding time delays are distributed from 0.09 s to 1.15 s. However, the start-time detected by WED (solid green and orange lines) is relatively robust to the ambient noise with a very close distance to the real start-time (dashed red line). Also, the corresponding time delays are significantly reduced and distributed from 0.0333 s to 0.1578 s. This observation can validate the robustness of the developed DPSDT method to the ambient noise.

For the total 23 bus faults separately simulated on each bus, the developed DPSDT method is run for each electrical signal. A total of 4,531 PMU-based events are detected to

TABLE IV
TIME DELAYS COMPARISON OF A FAULT EVENT ON BUS #101 USING DPSDT AND WED

Type of Time Delays		WED	DPSDT
Algorithm-Related Delay	Computational Delay [s]	0.0296	0.0264
	Processing Delay [s]	0.0114	0.0108
Total Time Delay [s]		0.079	0.0752
Estimated Start-Time of Event [s]		81.09	81.0333
Time Instant of Control Actions [s]		81.169	81.1085

form the empirical distributions. Fig. 13 shows the strokes statistics of 23 fault events. The mean magnitudes of up- and down-strokes are 0.8846 p.u. and 0.8785 p.u., respectively. The mean durations of up- and down-strokes are 0.2296 s and 0.2322 s, respectively. The up-stroke magnitude presents a higher peak than the down-stroke, and the up-stroke duration presents a lower peak than the down-stroke. Fig. 13 also shows the individual empirical distributions of the stroke magnitude and duration for each bus fault event (23 distributions and one averaging distribution in each sub-figure). Note that in each sub-figure the distribution shapes among various PMU channels present the consistency due to the same type of bus faults. Statistical results with quantiles of these distributions can be used to judge whether a PMU-based event is a bus-fault event or a non-bus-fault event. Fig. 14 shows the joint distributions of magnitude and duration for up- and down-strokes. The joint distributions of magnitude and duration show two clear clusters at the bottom right corner of each figure. It can be seen that there is less dependence between stroke magnitude and duration. The distinct mode of stroke magnitude is located in the range of 0.9–1.0 p.u., and the distinct mode of stroke duration is located in the range of 0–0.6 s. This information can also be statistically used to predefine the PMU event rules introduced in Section III-A.

E. Analysis of Time Delays

1) Algorithm-Related Delay: Taking the fault event on Bus #101 as an example, Table IV shows different types of time delays in the simulated Siemens PSS/E 23-bus system. The algorithm-related delay consists of the computational delay and the processing delay. Here, the computational delay is mainly caused by the computational time for running one algorithm, while the processing delay is caused by finding the end-time of the first stroke/interval. As can be seen, the computational time (delay) of both methods is in the range of 260–300 ms. Moreover, the computational delay caused by DPSDT is slightly smaller than that caused by WED. Also, the processing delay using DPSDT is slightly smaller than that using WED.

2) PMU Communication Delay: The PMU communication delay is mainly caused by the latency of fiber optic digital communication. The Bonneville Power Administration (BPA) system has reported the typical PMU communication delay as approximately 38 ms [32], [33]. In this paper, we assume that DPSDT and WED algorithms are with the same PMU communication delay, i.e., 0.038 s. The total time delay is the

TABLE V
NUMERICAL RESULTS USING WED AND DPSDT WITH AND WITHOUT CONSIDERING TIME DELAYS

Metrics		WED	DPSDT	Difference
W/O Time Delays	$ROLV$ [%]	52.17	0.00	52.17
	$ROLF$ [%]	60.87	0.00	60.87
	$MTMV$ [s]	0.5663	0.4275	0.1388
	$MTMF$ [s]	0.3446	0.2087	0.1359
With Time Delays	$ROLV$ [%]	78.26	39.13	39.13
	$ROLF$ [%]	100.00	17.39	**82.61**
	$MTMV$ [s]	0.6620	0.5540	0.1080
	$MTMF$ [s]	0.4489	0.3297	0.1192

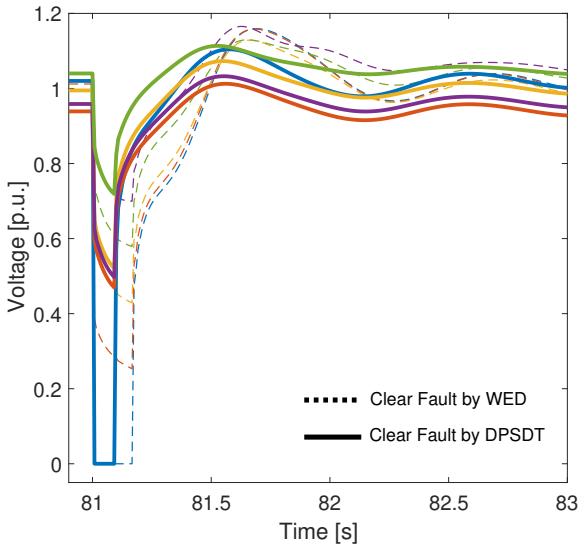

Fig. 15. Comparison of the fault clearance using WED and DPSDT on five representative buses considering time delays.

sum of the algorithm-related delay and the typical PMU communication delay. As shown in Table IV, the total time delays of DPSDT and WED are 0.079 and 0.0752, respectively.

3) Benefit Analysis Considering Time Delays: To evaluate the benefit of real-time control considering time-delays, the case study in Section V-D is performed. The real start-time of this event is preset at 81 s. The start-time of events using WED and DPSDT is estimated at 81.09 s and 81.0333 s, respectively. The time instant of real-time control actions is the sum of the estimated start-time of events and the total time delay. As shown in Table IV, after considering the total time delay, the real-time control actions using WED and DPSDT are applied on time instants of 81.169 s (=81.09+0.079) and 81.1085 s (=81.0333+0.0752), respectively.

Fig. 15 compares the fault clearance process using WED and DPSDT on five representative buses considering the impact of time delays. By using the control action time provided by DPSDT, bus faults can be cleared with more slight fluctuations for the voltage data. This observation is similar with that in Fig. 9 where time delays are not considered. For the sake of numerical analysis, Table V shows the metrics using WED and DPSDT with and without (W/O) considering time delays. As can be seen, for both cases with and without considering time delays, all the four metrics, including $ROLV$, $ROLF$, $MTMV$, and $MTMF$, are reduced due to using the more accurate start-time information provided by DPSDT. Particularly, there are not any buses with out-of-limit voltage and frequency using DPSDT, i.e., $ROLV$=0% and $ROLF$=0%. Another interesting finding is that all the four metrics are increased considering time delays. Also, this observation is consistent with that in Fig. 15.

TABLE VI
FAULT TYPES IDENTIFICATION

Fault Types	Abrupt Change on Voltage Data	Abrupt Change on Frequency Data
But Fault	✘	✘
Line Outage	–	✘
Generator Outage	✘	–

The benefits of using DPSDT are still very desirable even if time delays are considered. To evaluate this, the difference of metrics using WED and DPSDT are also calculated in Table V. For the difference of $ROLV$, $MTMV$, and $MTMF$, the benefits of using DPSDT are slightly reduced but still desirable when considering time delays. However, for the $ROLF$ metric, the benefit of using DPSDT is slightly increased from 60.87% to 82.16%. This is mainly because the overall buses violate the frequency limitation using WED when time delays are considered, i.e., $ROLF$=100%, while only 17.39% of buses are out-of-limit using DPSDT.

F. Fault Types Identification and Location

To identify the specific fault type and its location, one line outage and one generator outage are simulated on the Siemens PSS/E 23-bus system in Section V-D, respectively. The line outage is set on Line 151–152, and the generator outage is set on the generator connected with Bus 3018. The 23-bus system topology can be seen in [3]. Fig. 16 shows the results of NWE metrics for the voltage and frequency data with one line outage and one generator outage, respectively. For the line outage, there are several abrupt changes of NWE metrics in the frequency data, while the voltage data is without any abrupt change. For the generator outage, there are two abrupt changes of the voltage data on two buses: one connected with the generator and the other one connected with the corresponding transformer, while the frequency data is without any abrupt change. However, for the bus fault in Fig. 10, there is only one abrupt change in both frequency and voltage data. This finding can be used to identify the specific fault type as shown in Table VI.

By using the developed DPSDT method, the event can also be located. For the bus fault, there is only one abrupt change on the bus where the bus fault occurs. For the line outage, there is the largest difference between the NWE metrics of frequency data on Bus 151 and that on Bus 152 in Fig. 16b. This is mainly caused by the outage on Line 151–152. For the generator outage, there two abrupt changes of the NWE metric of voltage data on Bus 3018 and Bus 3008 in Fig. 16c. This is mainly caused by the outage of generator connected with Bus 3018.

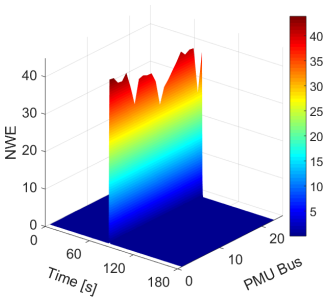

(a) Voltage data with an outage on Line 151–152

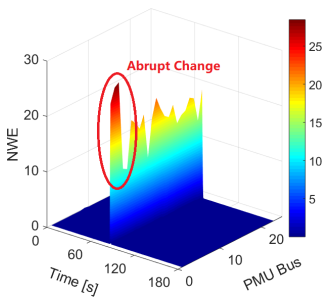

(b) Frequency data with an outage on Line 151–152

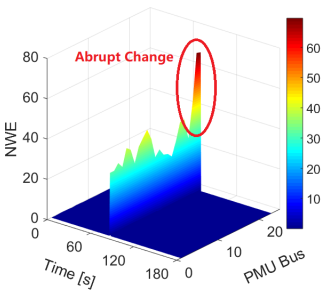

(c) Voltage data with an outage of generator connected on Bus 3018

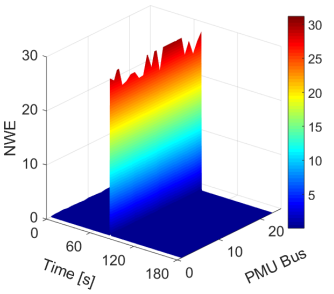

(d) Frequency data with an outage of generator connected on Bus 3018

Fig. 16. Comparison of NWE metrics for the voltage (left) and frequency (right) data with one line outage and one generator outage.

G. Impact of Thresholds on the Detection Accuracy for Different Types of Events

Fig. 17 compares the impacts of different thresholds with a fault on Bus #101 and an outage on Line 151–152. Three threshold coefficients ϕ_{mag} and ϕ_{slo} of -10%, 10%, and 50% are used to get different threshold values based on (3) and (4). As shown in Figs. 17a and 17b, the negative ϕ_{mag} and ϕ_{slo} (-10%) significantly impact the detection accuracy with five and four false alarm events for the bus fault and line outage, respectively. The appropriate ϕ_{mag} and ϕ_{slo} (10%) can detect the accurate events without any false alarm or missed events in Figs. 17c and 17d. However, when ϕ_{mag} and ϕ_{slo} increase to 50%, one upward stroke is missed in Fig. 17e, and both upward and downward strokes are missed in Fig. 17f. Compared with the bus fault, this is mainly because the line outage causes a relatively small oscillation of voltage, which is relatively sensitive to the thresholds of DPSDT.

VI. Conclusion

In this paper, we developed a novel PMU-based event detection method by using the swinging door trending (SDT) compression method and dynamic programming. The SDT method for data compression is first used to compress the real-time PMU data into multiple compression intervals by the tunable door width parameter. Then dynamic programming is utilized to solve an optimization problem, which is recursively constituted by a score function. Adjacent compression intervals with the same slope direction are merged and detected based on predefined PMU event rules. Compared with the conventional wavelet-based event detection (WED) method, the effectiveness of the developed dynamic programming based SDT (DPSDT) method is verified by numerical simulations on

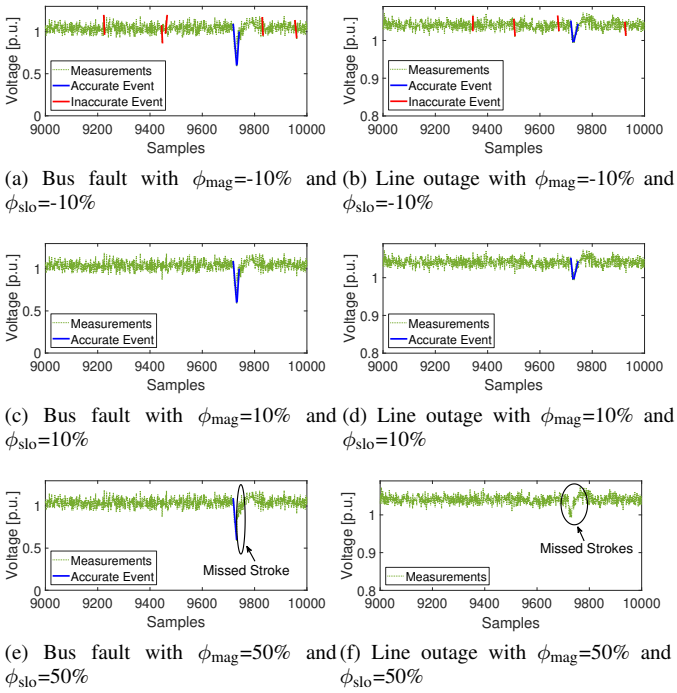

(a) Bus fault with ϕ_{mag}=-10% and ϕ_{slo}=-10%

(b) Line outage with ϕ_{mag}=-10% and ϕ_{slo}=-10%

(c) Bus fault with ϕ_{mag}=10% and ϕ_{slo}=10%

(d) Line outage with ϕ_{mag}=10% and ϕ_{slo}=10%

(e) Bus fault with ϕ_{mag}=50% and ϕ_{slo}=50%

(f) Line outage with ϕ_{mag}=50% and ϕ_{slo}=50%

Fig. 17. Comparison of the impacts of thresholds with a fault on Bus #101 (left) and an outage on Line 151–152 (right).

real and synthetic PMU data. Some observations are shown as follows:

(i) The developed method is able to clearly present the significant changes of both decomposition coefficients and the normalized wavelet energy (NWE) metric.

(ii) The detailed start-time and placement information of a PMU event can be precisely detected based on data of a high reporting rate using DPSDT.

(iii) PMU event features, including the magnitude and duration, are all characterized and fault events can be instantly cleared by using the developed DPSDT since the start-time of the event is precisely identified.

Acknowledgment

This work was authored in part by Alliance for Sustainable Energy, LLC, the Manager and Operator of the National Renewable Energy Laboratory for the U.S. Department of Energy (DOE) under Contract No. DE-AC36-08GO28308. Funding provided by the U.S. Department of Energy Grid Modernization Lab Consortium. The views expressed in the article do not necessarily represent the views of the DOE or the U.S. Government. The U.S. Government retains and the publisher, by accepting the article for publication, acknowledges that the U.S. Government retains a nonexclusive, paid-up, irrevocable, worldwide license to publish or reproduce the published form of this work, or allow others to do so, for U.S. Government purposes. In addition, the authors would like to thank the anonymous reviewers for their constructive suggestions to this research. The authors would also like to thank Dr. Yiwei Qiu and Dr. Linzhi Li from Zhejiang University in China for helping use the simulation software Siemens PSS/E, and Dr. Yang Li from Northeast Electric

Power University in China for the discussion of simulating the 23-bus system.

REFERENCES

[1] D. Anderson, C. Zhao, C. Hauser, V. Venkatasubramanian, D. Bakken, and A. Bose, "Real-time simulation for smart grid control and communications design," *IEEE Power Energy Mag.*, vol. 10, no. 1, pp. 49–57, 2012.

[2] Q. Dong, J. Sun, Q. Wu, and Y. Liu, "A method for filtering low frequency disturbance in PMU data before coordinated usage in SCADA," *IEEE Trans. Power Syst.*, vol. 32, no. 4, pp. 2810–2816, 2017.

[3] L. Xie, Y. Chen, and P. R. Kumar, "Dimensionality reduction of synchrophasor data for early event detection: Linearized analysis," *IEEE Trans. Power Syst.*, vol. 29, no. 6, pp. 2784–2794, 2014.

[4] S. S. Negi, N. Kishor, K. Uhlen, and R. Negi, "Event detection and its signal characterization in PMU data stream," *IEEE Trans. Ind. Inform.*, 2017, in press.

[5] D.-I. Kim, T. Y. Chun, S.-H. Yoon, G. Lee, and Y.-J. Shin, "Wavelet-based event detection method using PMU data," *IEEE Trans. Smart Grid*, vol. 8, no. 3, pp. 1154–1162, 2017.

[6] F. Zhang, L. Cheng, X. Li, Y. Sun, W. Gao, and W. Zhao, "Application of a real-time data compression and adapted protocol technique for WAMS," *IEEE Trans. Power Syst.*, vol. 30, no. 2, pp. 653–662, 2015.

[7] C. Ponce and D. Bindel, "FLiER: Practical topology update detection using sparse PMUs," *IEEE Trans. Power Syst.*, vol. 32, no. 6, pp. 4222–4232, 2017.

[8] H. Jiang, X. Dai, D. W. Gao, J. J. Zhang, Y. Zhang, and E. Muljadi, "Spatial-temporal synchrophasor data characterization and analytics in smart grid fault detection, identification, and impact causal analysis," *IEEE Trans. Smart Grid*, vol. 7, no. 5, pp. 2525–2536, 2016.

[9] S. You, Y. Liu, G. Kou, X. Zhang, W. Yao, Y. Su, S. Hadley, and Y. Liu, "Non-invasive identification of inertia distribution change in high renewable systems using distribution level PMU," *IEEE Trans. Power Syst.*, 2017, in press.

[10] T. Werho, V. Vittal, S. Kolluri, and S. M. Wong, "A potential island formation identification scheme supported by PMU measurements," *IEEE Trans. Power Syst.*, vol. 31, no. 1, pp. 423–431, 2016.

[11] J. E. Tate and T. J. Overbye, "Line outage detection using phasor angle measurements," *IEEE Trans. Power Syst.*, vol. 23, no. 4, pp. 1644–1652, 2008.

[12] Y. Liu, S. You, J. Tan, Y. Zhang, and Y. Liu, "Frequency response assessment and enhancement of the US power grids toward extra-high photovoltaic generation penetrations–an industry perspective," *IEEE Trans. Power Syst.*, vol. 33, no. 3, pp. 3438–3449, 2018.

[13] J. Zhao, J. Tan, L. Wu, L. Zhan, W. Yao, Y. Liu, J. R. Gracia, and P. D. Ewing, "Impact of measurement errors on synchrophasor applications," in *Proc. IEEE Power Energy Soc. Gen. Meeting*, Chicago, IL, USA, 2017, pp. 1–5.

[14] Y. Guo, K. Li, D. Laverty, and Y. Xue, "Synchrophasor-based islanding detection for distributed generation systems using systematic principal component analysis approaches," *IEEE Trans. Power Deliv.*, vol. 30, no. 6, pp. 2544–2552, 2015.

[15] P. H. Gadde, M. Biswal, S. Brahma, and H. Cao, "Efficient compression of PMU data in WAMS," *IEEE Trans. Smart Grid*, vol. 7, no. 5, pp. 2406–2413, 2016.

[16] P. Bhui and N. Senroy, "Application of recurrence quantification analysis to power system dynamic studies," *IEEE Trans. Power Syst.*, vol. 31, no. 1, pp. 581–591, 2016.

[17] M. Biswal, S. M. Brahma, and H. Cao, "Supervisory protection and automated event diagnosis using PMU data," *IEEE Trans. Power Deliv.*, vol. 31, no. 4, pp. 1855–1863, 2016.

[18] M. K. Jena, B. K. Panigrahi, and S. R. Samantaray, "A new approach to power system disturbance assessment using wide-area postdisturbance records," *IEEE Trans. Ind. Inform.*, vol. 14, no. 3, pp. 1253–1261, 2018.

[19] J. C. S. de Souza, T. M. L. Assis, and B. C. Pal, "Data compression in smart distribution systems via singular value decomposition," *IEEE Trans. Smart Grid*, vol. 8, no. 1, pp. 275–284, 2017.

[20] E. H. Bristol, "Swinging door trending: adaptive trend recording?" in *Proc. ISA National Conf.*, 1990, pp. 749–753.

[21] N. G. Boulaxis and M. P. Papadopoulos, "Optimal feeder routing in distribution system planning using dynamic programming technique and GIS facilities," *IEEE Trans. Power Deliv.*, vol. 17, no. 1, pp. 242–247, 2002.

[22] R. Sevlian and R. Rajagopal, "Detection and statistics of wind power ramps," *IEEE Trans. Power Syst.*, vol. 28, no. 4, pp. 3610–3620, Nov. 2013.

[23] M. Cui, D. Ke, Y. Sun, D. Gan, J. Zhang, and B.-M. Hodge, "Wind power ramp event forecasting using a stochastic scenario generation method," *IEEE Trans. Sustain. Energy*, vol. 6, no. 2, pp. 422–433, Apr. 2015.

[24] M. Cui, J. Zhang, A. R. Florita, B.-M. Hodge, D. Ke, and Y. Sun, "An optimized swinging door algorithm for identifying wind ramping events," *IEEE Trans. Sustain. Energy*, vol. 7, no. 1, pp. 150–162, Jan. 2016.

[25] R. Preece and J. V. Milanović, "Risk-based small-disturbance security assessment of power systems," *IEEE Trans. Power Deliv.*, vol. 30, no. 2, pp. 590–598, 2015.

[26] F. Teng, Y. Mu, H. Jia, J. Wu, P. Zeng, and G. Strbac, "Challenges on primary frequency control and potential solution from EVs in the future GB electricity system," *Appl. Energy*, vol. 194, pp. 353–362, 2017.

[27] The Texas Synchrophasor Network. [Online]. Available: https://web.ecs.baylor.edu/faculty/grady/Texas_Synchrophasor_Network.html

[28] A. Sant, W. M. Grady, S. Santoso, and J. Ramos, "A screening procedure to detect significant power system events recorded by the texas synchrophasor network," in *Proc. IEEE Power Energy Soc. Gen. Meeting*, San Diego, CA, USA, 2012, pp. 1–5.

[29] Siemens. (2010) PSSE 32.0.5 Program Operational Manual.

[30] M. K. Neyestanaki and A. Ranjbar, "An adaptive PMU-based wide area backup protection scheme for power transmission lines," *IEEE Trans. Smart Grid*, vol. 6, no. 3, pp. 1550–1559, 2015.

[31] T. Wang, A. Pal, J. S. Thorp, Z. Wang, J. Liu, and Y. Yang, "Multi-polytope-based adaptive robust damping control in power systems using CART," *IEEE Trans. Power Syst.*, vol. 30, no. 4, pp. 2063–2072, 2015.

[32] H. Wu, K. S. Tsakalis, and G. T. Heydt, "Evaluation of time delay effects to wide-area power system stabilizer design," *IEEE Trans. Power Syst.*, vol. 19, no. 4, pp. 1935–1941, 2004.

[33] C. W. Taylor, M. V. Venkatasubramanian, Y. Chen *et al.*, "Wide-area stability and voltage control," in *Proc. 7th Symp. Specialties Electr. Oper. Expansion Planning*, 2000, pp. 21–26.

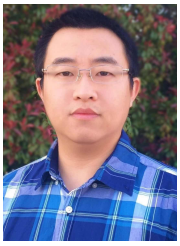

Mingjian Cui (S'12–M'16–SM'18) received the B.S. and Ph.D. degrees from Wuhan University, Wuhan, Hubei, China, all in Electrical Engineering and Automation, in 2010 and 2015, respectively.

Currently, he is a Postdoctoral Research Associate at Southern Methodist University, Dallas, Texas, USA. He was a Postdoctoral Research Associate at the University of Texas at Dallas, Richardson, Texas, USA, in 2016 and 2017. He was also a Visiting Scholar from 2014 to 2015 in the Transmission and Grid Integration Group at the National Renewable Energy Laboratory (NREL), Golden, Colorado, USA. His research interests include power system operation, wind and solar forecasts, machine learning, data analytics, and statistics. He has published over 50 journal and conference papers.

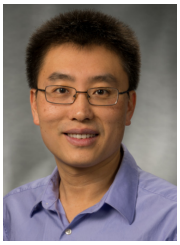

Jianhui Wang (M'07–SM'12) received the Ph.D. degree in electrical engineering from Illinois Institute of Technology, Chicago, Illinois, USA, in 2007.

Presently, he is an Associate Professor with the Department of Electrical Engineering at Southern Methodist University, Dallas, Texas, USA. Prior to joining SMU, Dr. Wang had an eleven-year stint at Argonne National Laboratory with the last appointment as Section Lead – Advanced Grid Modeling. Dr. Wang is the secretary of the IEEE Power & Energy Society (PES) Power System Operations, Planning & Economics Committee. He has held visiting positions in Europe, Australia and Hong Kong including a VELUX Visiting Professorship at the Technical University of Denmark (DTU). Dr. Wang is the Editor-in-Chief of the IEEE Transactions on Smart Grid and an IEEE PES Distinguished Lecturer. He is also the recipient of the IEEE PES Power System Operation Committee Prize Paper Award in 2015.

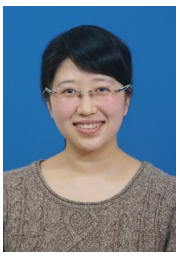

Jin Tan (S'11–M'15) received the B.E. and Ph.D. degree in electrical engineering from Southwest Jiaotong University, Chengdu, China, in 2007 and 2014, respectively.

From 2009 to 2011, she was a visiting Ph.D. student at Department of Energy Technology, Aalborg University, Denmark. In 2014, she was a postdoc researcher in the Department of Electrical Engineering and Computer Science, University of Tennessee, Knoxville, TN, USA. Currently, she is a research engineer with the power system engineering center, National Renewable Energy Laboratory, Golden, CO, USA. Her research interests include power system stability with large-scale renewable integration, dynamic modeling of various renewable generation, ancillary control of renewable integration, and energy storage for grid application.

Anthony R. Florita (M'13) is a Senior Research Engineer within the Power Systems Engineering Center, National Renewable Energy Laboratory, Golden, CO, USA. His current research involves building-to-grid modeling and simulation, short-term weather forecasting for model predictive control, and probabilistic state estimation for decision support. His general research interests include multidisciplinary design optimization, causal Bayesian networks, and renewable systems integration. He has authored/coauthored more than 50 peer-reviewed publications in these areas.

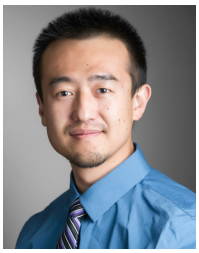

Yingchen Zhang (M'07–SM'16) received the B.S. degree from Tianjin University, Tianjin, China, in 2003, and the Ph.D. degree from Virginia Polytechnic Institute and State University, Blacksburg, VA, USA, in 2010.

Currently, he is a principal researcher and manager of the sensing and predictive analytics group at the National Renewable Energy Laboratory. He is also a visiting research assistant professor at the University of Denver and an adjunct faculty at Colorado State University. He has over 10 years of experience in power industry in the areas of data analytics for power systems, renewable integration, energy management systems. He authored/coauthored over 80 peer reviewed publications and holds one U.S. patent. His key areas of expertise lie in predictive analytics for energy systems, advanced energy management system for future grids, and the impact of large-scale integration of renewable energies on power system operations. Dr. Zhang serves as an editor for the IEEE Transactions on Sustainable Energy.